JOURNAL OF SPACECRAFT AND ROCKETS
Vol. 36, No. 1, January–February 1999

# Computational Simulation Improvements of Supersonic High-Angle-of-Attack Missile Flows

Eswar Josyula*
*U.S. Air Force Research Laboratory, Wright–Patterson Air Force Base, Ohio 45433-7913*

**A numerical simulation is presented for the steady-state flow over a missile body configuration for supersonic Mach number at incidence. The missile has a diameter $d$ of 0.09398 m and a length of 13$d$. Flow conditions specified are Mach 2.5, angle of attack 14 deg, and Reynolds number $1.23 \times 10^6$ based on the diameter of afterbody to match experimental conditions. The three-dimensional Navier–Stokes equations in mass-averaged form were numerically integrated using both central and upwind difference methods, implicit Beam and Warming algorithm with the two-equation $k$–$\epsilon$ turbulence model to provide closure of the system of equations. The upwind method captured the crossflow shock better, and the central difference method predicted the vortex shape and strength better. Modifications to the two-equation turbulence model, which limited the production of eddy viscosity for vortical flows, were implemented to assess the improvement in accuracy. The modifications improved prediction of the vortical shape and strength and showed improvements in the surface pressure predictions due to stronger primary and secondary vortices. A grid resolution study to examine the effects of the modifications to the $k$–$\epsilon$ turbulence model was conducted. The grid study indicated that the improvements in the shear layer resolution and vortex core predictions were better when refinement was made in the body normal and circumferential directions.**

## Nomenclature

| | |
|---|---|
| $d$ | = diameter of cylindrical afterbody, 0.09398 m |
| $k$ | = nondimensional turbulence kinetic energy |
| $P_k$ | = nondimensional turbulence production source term |
| $p_t$ | = nondimensional total pressure |
| $Re$ | = reference Reynolds number, $\rho_\infty u_\infty c/\mu_\infty$ |
| $\|s\|$ | = nondimensional strain rate |
| $x, y, z$ | = nondimensional Cartesian coordinates in streamwise, vertical, and lateral directions |
| $\alpha$ | = angle of attack, deg |
| $\epsilon$ | = nondimensional turbulence energy dissipation |
| $\mu, \mu_t$ | = molecular and turbulent viscosity coefficients |
| $\xi, \eta, \zeta$ | = computational coordinates |
| $\rho$ | = nondimensional fluid density |
| $\phi$ | = circumferential angle on body measured from windward side, deg |
| $\omega$ | = nondimensional vorticity |
| $\infty$ | = freestream value |

## Introduction

AT supersonic Mach numbers the flowfields around missile body configurations at angle of attack have boundary-layer separation resulting in the development of vortical structures. The crossflow separation on the leeward side is characterized by the crossflow separation line and the strength of the vortex, which develops from the separation. Prediction of these quantities by computational methods in recent years are enhanced by improved algorithms and by making improvements in the available turbulence models.

There have been a number of numerical studies in recent years dealing with the problem of vortical flows for ogive-cylinder configurations at angle of attack.[1–5] The importance of radial grid resolution for the attached turbulent viscous layers and the radial and circumferential resolution of the leeward vortices was noted.[1] The work used the algebraic eddy-viscosity model of Baldwin and Lomax[6] and modifications[1] were made to the turbulence model to properly evaluate the viscous-layer scale length under the leeward vortex structure. The computational work of Borrel et al.[2] also used the algebraic eddy-viscosity model[1,6] and noted the problem of determining the mixing length at 20-deg incidence. Moran and Beran[4] also used the algebraic turbulence model, made modifications to account for compressibility and pressure gradients, and also altered the two coefficients in the outer region to better match the law of the wake.

A collaborative study[5] with participants from Canada, the United Kingdom and the United States applied several Navier–Stokes codes with algebraic and two-equation turbulence models to predict the flow about a missile body configuration for transonic and supersonic speeds at 8- and 14-deg angle of attack for which detailed experimental data are available. The present work considers one of the cases of Ref. 5 to assess improvements in prediction accuracy of vortical shape and strength. This study comprises numerical solutions of the Navier–Stokes equation with the $k$–$\epsilon$ turbulence model for supersonic flow past a missile body configuration at incidence. To limit the excessive values of eddy viscosity produced by the standard $k$–$\epsilon$ turbulence model in vortical flows, the modifications to the turbulent kinetic energy proposed by Menter[7] and Dacles-Marianiet al.[8] were used in the present study. These modifications to the turbulence model used for subsonic vortical flows by Gordnier[9] over delta wings resulted in improved computational simulation, when compared with the experimental mean flow measurements. Gordnier's[9] grid resolution studies with modifications, although not fully conclusive, showed larger values of eddy viscosity for the refined grid, but with little effect on the computed vortical solution in the $\alpha = 15$ deg case. However, only relatively small changes in the level of eddy viscosity occurred in the boundary-layer region under the primary vortex. Showing the effects of the modification to the turbulence model on supersonic vortical flows is one of the objectives of the present study. A grid resolution study using the unmodified and modified turbulence model is conducted. Two different numerical algorithms, namely central and upwind difference, are also compared to assess the effects of the algorithm chosen on the computed flowfield.

## Analysis

This section gives details of fluid dynamic equations and turbulence model of an existing computer code, FDL3DI, developed in the U.S. Air Force Research Laboratory. The governing equations were taken to be the unsteady, three-dimensional, compressible, mass-averaged Navier–Stokes equations. The $k$–$\epsilon$ turbulence model is that of Jones and Launder[10,11] for which the generalized formulation was written by Gerolymos.[12] The model incorporates

Presented as Paper 98-0525 at the AIAA 36th Aerospace Sciences Meeting, Reno, NV, Jan. 12–15, 1998; received Feb. 9, 1998; revision received Aug. 18, 1998; accepted for publication Sept. 10, 1998. 

*Research Aerospace Engineer, Computational Sciences Branch. Senior Member AIAA.

low Reynolds number terms to account for near-wall effects. The turbulence model is implemented with the compressibility correction of Sarkar et al.[13] for more accurate representationof supersonic flows. Two modifications to the turbulent kinetic energy production term were used by Gordnier.[9] The first, proposed by Menter,[7] limits the production term:

$$P_k = \min(P_k, 20.0\rho\epsilon) \tag{1}$$

The standard production term in $k$–$\epsilon$ equations can be written in Cartesian form:

$$P_k = \frac{\mu_t}{Re}\left[|s|^2 - \frac{2}{3}\left(\frac{\partial u_k}{\partial x_k}\right)^2\right] \tag{2}$$

where $|s| = \sqrt{(2S_{ij}S_{ij})}$ is the strain rate. The second modification, first proposed by Dacles-Mariani et al.,[8] replaced the $|s|$ in the production term by the expression, $|\omega| + 2\min(0, |s| - |\omega|)$. The advantage of this formulation is that it reduces eddy viscosity in regions of the flow where vorticity exceeds the strain rate, such as in the vortex core. This modification should have negligible effect in shear layers where $|s|$ and $|\omega|$ are similar. The complete description of the governing equations appears in Ref. 14.

The mass-averaged Navier–Stokes equations are solved using a numerical code based on the implicit Beam and Warming algorithm.[15] The algorithm is second-order accurate spatially and uses a blended second- and fourth-order Jameson-type damping.[16] The MUSCL-based Roe approximate Riemann solver[17] is also available in the present code. A limiter was employed to stabilize the solution near shocks, and a flow- and mesh-based cutoff applied to the two nonlinear eigenvalues in each direction to enforce the entropy condition. The equations solved by the Beam and Warming algorithm were used successfully in analyzing vortex breakdown above a pitching delta wing by Visbal[18] and turbulent cylinder juncture flows by Rizzetta.[19]

## Boundary Conditions

Because supersonic conditions exist at both the inflow and outflow, at the inflow, freestream conditions were applied, and at the outflow, flow variables were extrapolated from the interior. Along the far-field boundary, freestream conditions were specified. For the body surfaces, no slip was applied, zero normal pressure gradient, and an adiabatic wall was used. A line of singularity in the coordinate transformation lies along the longitudinal axis and extends from the tip of the forebody to the upstream far-field boundary. The flow variables on this line was obtained by extrapolating the conserved variables to the surface and then performing the appropriate averaging of these values. The flow was assumed to have bilateral symmetry with respect to the $x$–$y$ plane; therefore $w = 0$ and $\partial/\partial\zeta = 0$ for all of the remaining variables on the symmetry boundary. For the $k$–$\epsilon$ equations, freestream values of $k$ and $\epsilon$ were specified at the far-field boundaries. The freestream value of $k_\infty$ was obtained by defining a freestream turbulence intensity, $T_i$ as $T_i = [2/3k_\infty]^{1/2}/u_\infty$. The value of $T_i$ was assumed to be $T_i = 0.005$. A corresponding value of $\epsilon_\infty$ was then determined by assuming $\mu_{t_\infty} = \mu_\infty$. The values of $k$ and $\epsilon$ were set to zero at the surface. All other boundary conditions on $k$ and $\epsilon$ were specified in a manner similar to the flow variables.

## Conditions of Numerical Simulation

The experimental data were provided by the Defence Research Agency of the United Kingdom as given in Ref. 5. The geometry consists of a length of 13 diameters, as shown in Fig. 1. The nose is given by the equation $r(x)/d = -0.002615(x/d)^3 - 0.03986(x/d)^2 + 0.30984(x/d)$. The test case chosen for this study has freestream conditions of Mach number 2.5, angle of attack 14 deg, Reynolds number $1.23 \times 10^6$ based on the diameter of the afterbody of 0.09398 m, total pressure 141,827 N/m$^2$, and total temperature 308 K. The experimental data consist of surface pressure measurements at 32 axial locations and pitot pressure probe sweeps of the flowfield at axial locations of $5.5d$ and $11.5d$.

**Table 1 Details of flow conditions for Mach number = 2.5, AOA = 14 deg, and $Re_d = 1.23 \times 10^6$ and grids considered**

| $\Delta_n$[a] | Grid size[b] | Memory, megawords |
|---|---|---|
| 0.00003 | $100 \times 50 \times 51$ | 10 |
| 0.00003 | $150 \times 75 \times 76$ | 33 |
| 0.00001 | $121 \times 89 \times 89$ | 37 |
| 0.000005 | $121 \times 159 \times 159$ | 115 |

[a]Minimum normal grid spacing normalized by $d = 0.09398$ m.
[b]Axial × radial × circumferential.

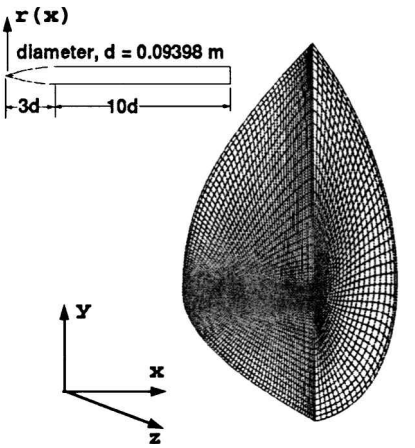


**Fig. 1 Body geometry and computational grid.**

Figure 1 also shows the computational grid used. The asymmetry in the grid allows for better resolution of the vortices on the leeward side and the strong shock close to the body on the windward side. The grids developed for this study are of the C type. Because flow symmetry is assumed, only a half grid in the circumferential direction was used.

Convergence to steady state was monitored by observing the integrated normalized surface pressure. The variation of eddy viscosity downstream of the body was also monitored over five characteristic times. The data processing rate (DPR) was $2.03 \times 10^{-5}$ CPU-s/point/iteration for the $121 \times 89 \times 89$ grid on a single processor of a C-90 computer for the turbulent calculation using the central difference method. The computer memory requirement for all cases is summarized in Table 1. To assess the accuracy of computational predictions of the strength of the pair of vortical structures on the missile body configuration, pitot pressure values were extracted and compared along lines in the horizontal H–H and vertical V–V directions traversing the vortex core (Figs. 2 and 3). These types of comparisons were adopted due to the availability of experimental pitot pressures at $x/d = 5.5$ and 11.5 in the flowfield. The core was identified by a point in the vortex where the minimum pitot pressure exists.

A grid size study was conducted to determine the effects of grid resolution on the computational results. The grid sizes and minimum distances for all four grids are given in Table 1. For the purpose of the grid study, the standard $k$–$\epsilon$ equations were used to model turbulence. The pitot pressure along the line (H–H) through the vortex core for the four grids is shown at an $x/d$ location of 11.5 in Fig. 2. It is seen that as the points in the radial and circumferential direction are increased, the solution reaches grid independence over most of the domain plotted. Although the finer grids ($121 \times 89 \times 89$ and $121 \times 159 \times 159$) demonstrate grid convergence for minimum pressure in the vortex core, the finest grid resolves the shear layer region better than other grids resulting in the second peak observed in Fig. 2. Figure 3 shows very small variation in the pitot pressure along the line (V–V) through the vortex core for the finer ($121 \times 89 \times 89$) and finest ($121 \times 159 \times 159$) grids. The surface pressure comparison for three of the grids demonstrating grid convergence is shown in Fig. 4, $x/d = 11.5$.

In subsequent discussions, the finer grid ($121 \times 89 \times 89$) was used to compare the solutions given by the two differencing methods,

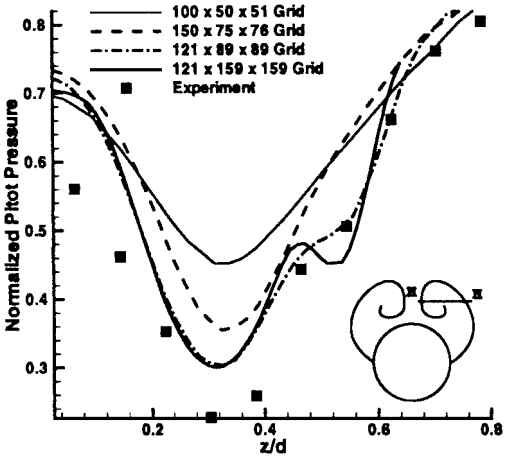


**Fig. 2 Grid study: comparison of pitot pressure along H–H traversing the vortex core, $x/d = 11.5$.**

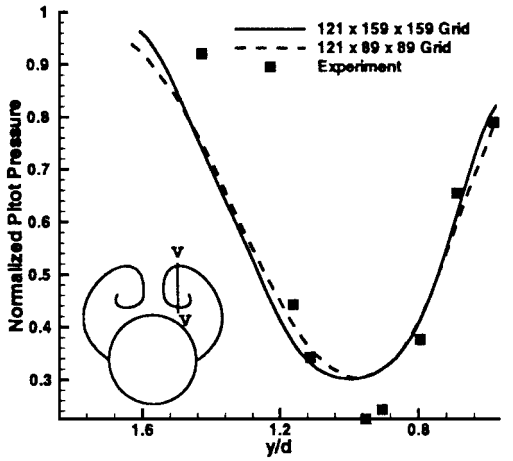


**Fig. 3 Grid study: comparison of pitot pressure along V–V traversing the vortex core, $x/d = 11.5$.**

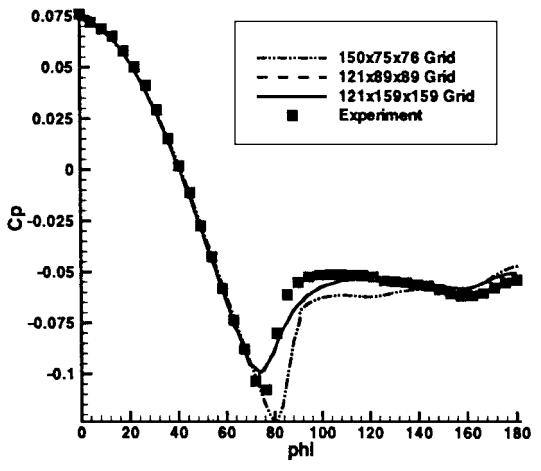


**Fig. 4 Grid study: comparison of surface pressure at $x/d = 11.5$.**

central and upwind. The finest grid ($121 \times 159 \times 159$) was used to study the effect of the modification to the turbulence model. A grid resolution study showing the effects of grids on the modification was done for the finer ($121 \times 89 \times 89$) and the finest ($121 \times 159 \times 159$) grids. The summary shown in Table 2 gives the cases considered.

## Results and Discussion

Results are given in two sections. The first section presents computational results for the two types of spatial discretization: 1) central differences for both inviscid and viscous terms and 2) upwind differences for inviscid terms and central differences for the viscous terms. The computations in this section use the standard $k$–$\epsilon$ equations to model effects of turbulence in the flowfield. The second section presents results for the effects of the modifications to the $k$–$\epsilon$ turbulence model on the flowfield.

**Table 2 Cases considered**

| Grid size | Type inviscid discretization | Modification to turbulence model |
|---|---|---|
| $121 \times 89 \times 89$ | Upwind | No |
| $121 \times 89 \times 89$ | Central | No |
| $121 \times 89 \times 89$ | Central | Yes |
| $121 \times 159 \times 159$ | Central | No |
| $121 \times 159 \times 159$ | Central | Yes |

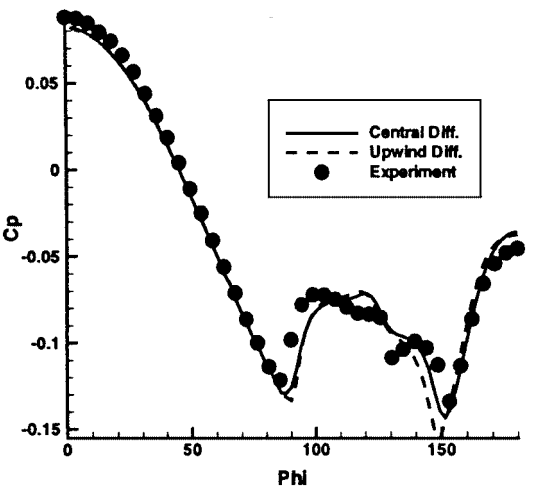


**Fig. 5 Comparison of surface pressure at $x/d = 6.5$.**

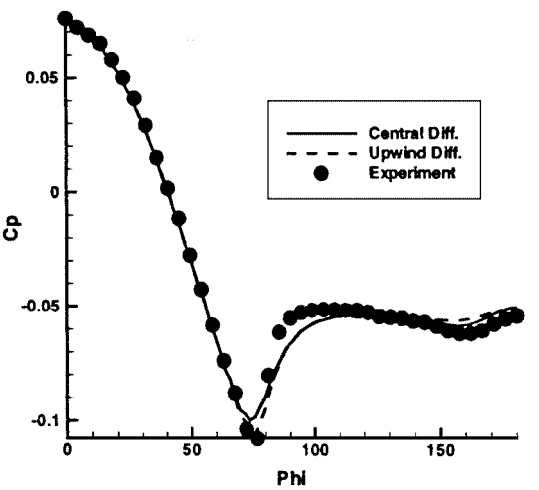


**Fig. 6 Comparison of surface pressure at $x/d = 11.5$.**

### Comparison of Central and Upwind Methods

The computations for the purpose of comparing the two methods were performed on a mesh consisting of $121 \times 89 \times 89$ nodes, in the axial $\times$ radial $\times$ circumferential directions using the standard $k$–$\epsilon$ turbulence model. Figures 5 and 6 show comparisons of the computed and experimental surface pressures vs circumferential angle $\phi$ measured from the windward side. The comparisons are for the central and upwind difference methods at axial stations $x/d = 6.5$ and 11.5. The surface pressure comparison up to $x/d = 6.5$ did not show any difference between the two methods. The surface pressure peak between $\phi = 90$–100 deg is displaced for the computational predictions of both methods for $x/d = 3.5$, 4.5, 5.5, and 6.5. Results for $x/d = 3.5$, 4.5, and 5.5 are shown in Ref. 14. The surface pressure comparison at $x/d = 6.5$ is shown in Fig. 5, which shows the

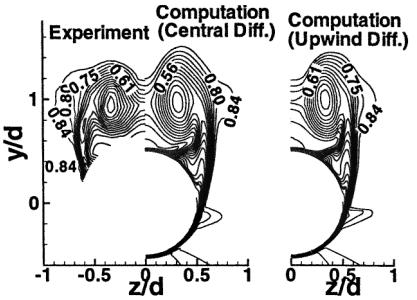


**Fig. 7 Comparison of pitot pressure at $x/d$ = 11.5 using central and upwind differencing.**

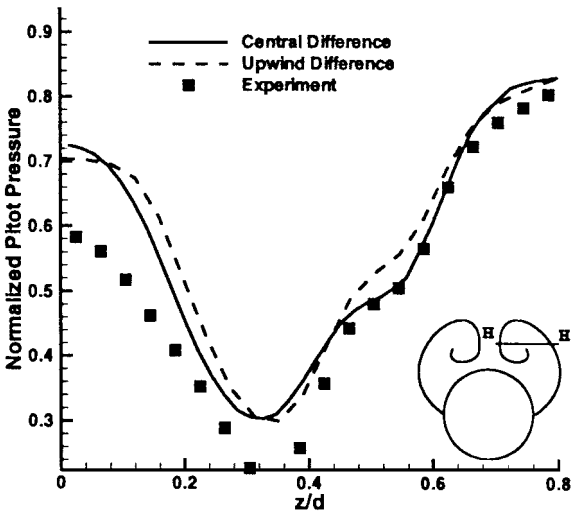


**Fig. 8 Comparison of pitot pressure along H–H traversing the vortex core, $x/d$ = 11.5.**

typical displacement at $\phi = 90$ deg. This displacement is a result of variation in location of the crossflow shock caused by the rapid expansion of the flow from the windward to the leeward side.

At $x/d = 11.5$, the upwind method predicts the $Cp$ peak better at $\phi = 73$ deg (Fig. 6), which is attributed to a stronger crossflow shock, than the central difference method. The overprediction of $Cp$ at this location of $x/d = 11.5$, $\phi = 73$ deg by the central difference method is about 6%. However, the pressure recovery on the surface, as a result of the compression of fluid behind the crossflow shock, is displaced the same for both methods when compared to the experimentally observed $Cp$ variation. The suction peak near $\phi = 150$ deg on the surface is better predicted by the central difference method at $x/d = 6.5$ (Fig. 5), attributable to a better defined primary vortex discussed subsequently. The surface pressures at $x/d = 7.5$ and 8.5 display similar behavior as discussed for $x/d = 6.5$ and are shown in Ref. 14.

Comparison of pitot pressure contours, at $x/d = 11.5$ (Fig. 7) and pitot pressure along the line (H–H) through the vortex core (Fig. 8) show details of the vortical flow structure for the experimental observations and computational predictions. It is clearly seen in comparison to the experimental pitot pressure contours that the vortex shape predicted by the central difference method is less elongated than that by the upwind method. Comparison of pitot pressure along the line (H–H) through the vortex core show that both differencing methods overpredict the pitot pressure at $z/d = 0$ (Fig. 8). This can be attributed to the elongation of the vortex (worse for the upwind method) seen in the pitot pressure contours (Fig. 7). This elongation of the vortex by both methods is due to the excess dissipation of the $k$–$\epsilon$ turbulence model.

### Effect of Modification to Turbulence Model

From the results just described, it appears that the standard $k$–$\epsilon$ turbulence model produces excessive values of eddy viscosity in regions of vortices away from the body for high-angle-of-attack missile flows. Results obtained by modifications to the turbulence model as presented in the Analysis section earlier are compared to results of the unmodified case. Comparisons of flowfield properties of eddy viscosity, $x$ component of vorticity, pitot pressure, and surface pressures are shown in this section. The central difference method was used for all of the cases presented in this section. A mesh size of 121 × 159 × 159 nodes in the axial × radial × circumferential directions was used for performing computations for the purpose of comparing the effects of modification to the turbulence model.

Locations of $x/d = 7.5$ and 11.5 are chosen to compare eddy viscosity produced by the unmodified and modified turbulence models (Fig. 9). At both locations it can be seen that the eddy viscosity is reduced by about half in the vortex region in the modified case. In the unseparated boundary layer on the windward side, however, the eddy viscosity produced by the two models is similar. The contours of the $x$ component of vorticity are shown for the unmodified and modified cases in Figs. 10 and 11. A larger and a better-defined secondary vortex at $x/d = 7.5$ is seen for the modified case (Fig. 10). This larger secondary vortex moves the primary vortex farther outward. The vorticity contours at $x/d = 11.5$ show a less elongated vortex shape for the modified than the unmodified case (Fig. 11). These improvements can be attributed to the lowering of the excess dissipation predicted by the modified turbulence model.

The effect of the modification is shown by the pitot pressure contours at $x/d = 5.5$ in Fig. 12. The contours are similar for the experiment and the computation with the modified turbulence model. The pitot pressure comparisons of the unmodified and modified turbulence models show similar behavior with the exception of the formation of a stronger secondary vortex predicted by the modified turbulence model. This stronger secondary vortex moves the primary vortex farther away from the body, thereby displacing the crossflow shock for the modified computation more toward the windward side.

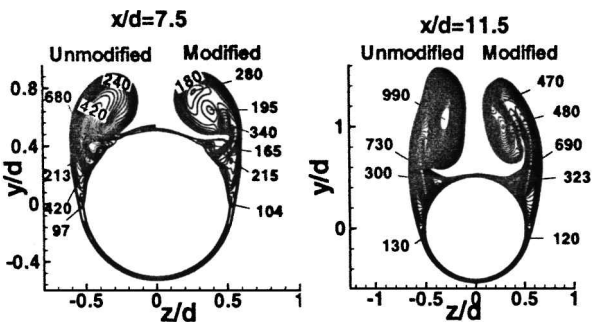


**Fig. 9 Comparison of eddy viscosity contours at $x/d$ = 7.5 and 11.5, $\Delta\mu_t$ of contours = 20.**

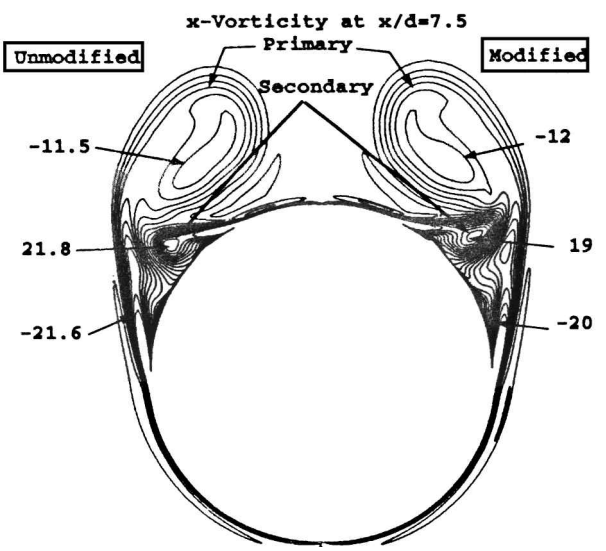


**Fig. 10 Comparison of $X$ vorticity contours at $x/d$ = 7.5, $\Delta\omega_x$ of contours = 2.1.**

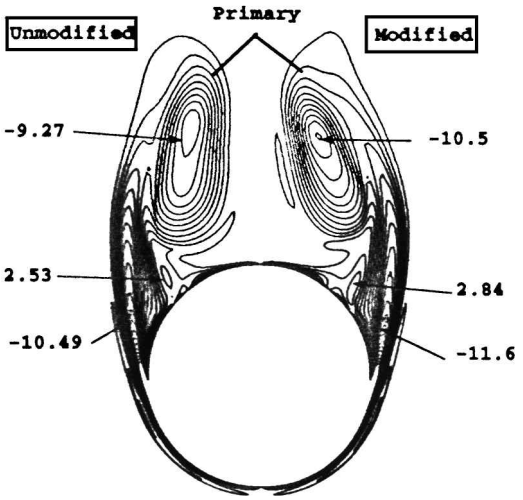


**Fig. 11 Comparison of $X$ vorticity contours at $x/d = 11.5$, $\Delta\omega_x$ of contours = 2.1.**

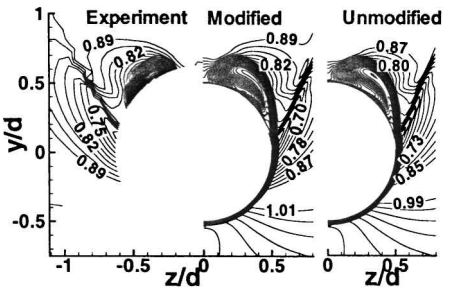


**Fig. 12 Comparison of pitot pressure contours at $x/d$ = 5.5 showing effect of modification to turbulence model.**

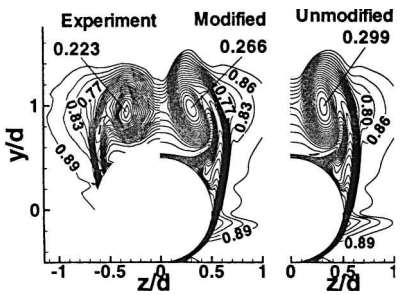


**Fig. 13 Comparison of pitot pressure contours at $x/d$ = 11.5 showing effect of modification to turbulence model.**

The comparison of pitot pressure contours at $x/d = 11.5$ for the unmodified and modified cases (Fig. 13) shows the vortical structure in the modified case with a rounded vortex due to reduced diffusivity of the turbulence model. The comparison of the computed pitot pressure contours with data at $x/d = 11.5$ for the unmodified and modified models clearly shows that the vortex core is better predicted by the modified model (19% overprediction) than the unmodified (34% overprediction) (Fig. 13). Figures 14 and 15 display pitot pressure variation along the lines (H–H) and (V–V) through the vortex core for the unmodified and modified turbulence models at $x/d = 11.5$, respectively. Figures 14 and 15 show that the modified model predicts more accurate low pressure in the core of the vortex as a result of the stronger vortex created due to reduced eddy viscosity. The prediction of the shear layer given by the pitot pressure peak at $z/d = 0.55$ (Fig. 14) is better for the modified model.

Figures 16–22 show comparisons of surface pressure in the circumferential direction at various axial locations for both unmodified and modified turbulence models with experimental data. The pressure peaks between $\phi = 70$–$120$ deg at all axial locations are lower for the modified model, a consequence of the displacement of the crossflow shock due to modifications, e.g., see Fig. 12. This surface pressure peak near $\phi = 100$ deg at $x/d = 3.5, 4.5, 5.5$, and 6.5 is predicted more accurately by the modified model (Figs. 16–19). The lowering of the eddy viscosity in the vortex increases the strength of the primary and secondary vortices, thereby displacing the shear layer separating from the missile body and, correspondingly, the crossflow shock.

The surface pressure peak influenced by the primary vortex at $\phi = 150$ deg is underpredicted by both models up to $x/d = 5.5$ (Figs. 17 and 18). At $x/d = 7.5$ (Fig. 20), there is a considerably

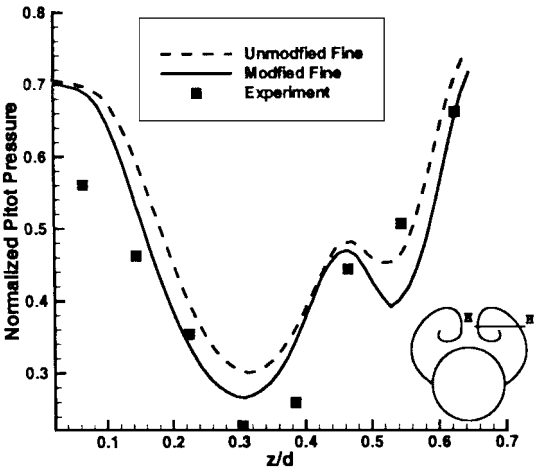


**Fig. 14 Comparison of pitot pressure along H–H traversing the vortex core, $x/d$ = 11.5.**

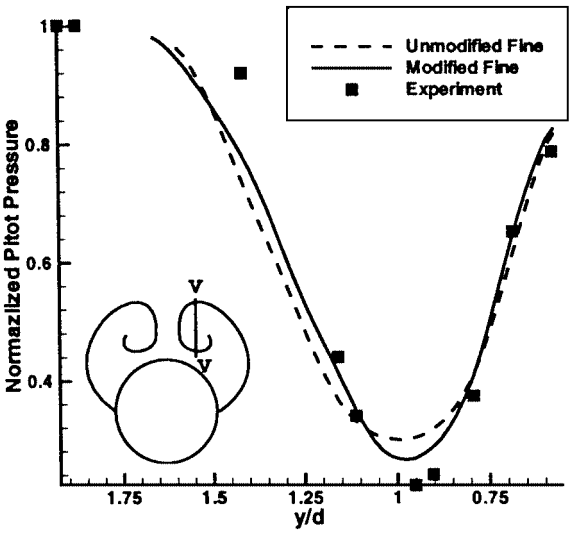


**Fig. 15 Comparison of pitot pressure along V–V traversing the vortex core, $x/d$ = 11.5.**

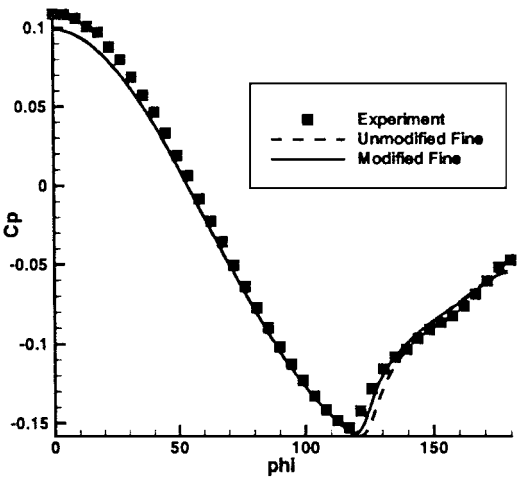


**Fig. 16 Comparison of surface pressure at $x/d$ = 3.5.**

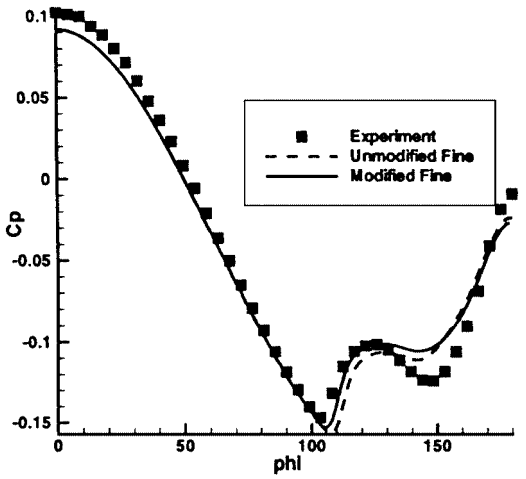


Fig. 17 Comparison of surface pressure at $x/d = 4.5$.

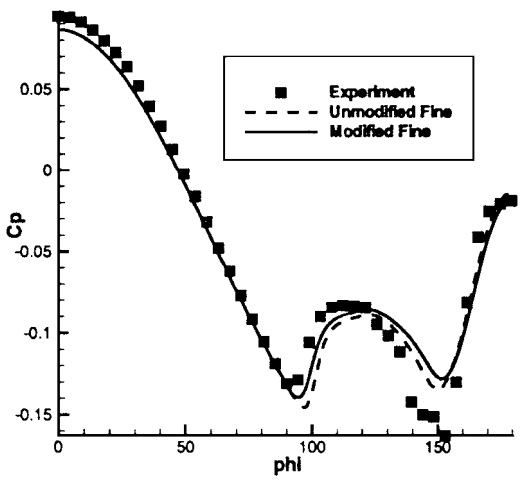


Fig. 18 Comparison of surface pressure at $x/d = 5.5$.

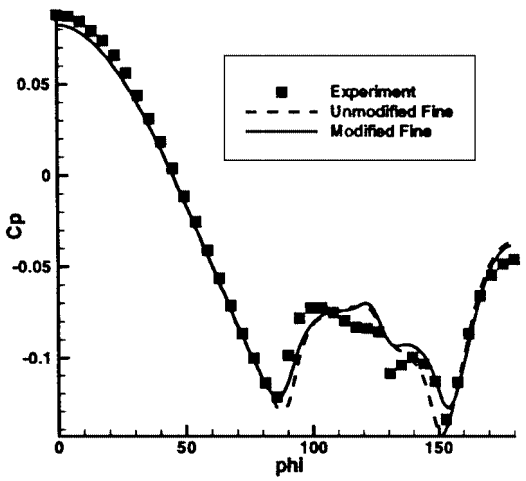


Fig. 19 Comparison of surface pressure at $x/d = 6.5$.

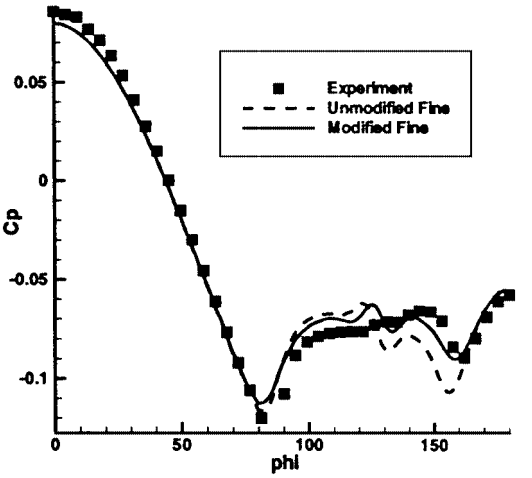


Fig. 20 Comparison of surface pressure at $x/d = 7.5$.

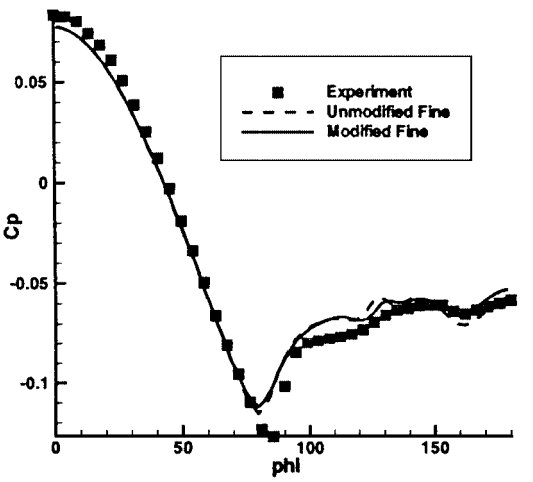


Fig. 21 Comparison of surface pressure at $x/d = 8.5$.

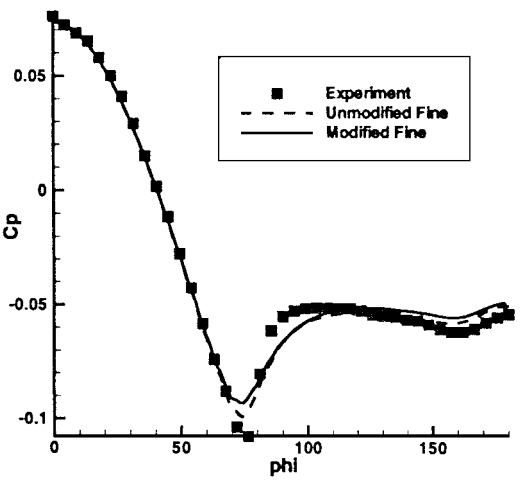


Fig. 22 Comparison of surface pressure at $x/d = 11.5$.

better agreement of the surface pressure at the $\phi = 150$ deg location with experimental data using the modified model, the improvement attributable to a better prediction of the primary vortex location and strength. This peak computed by the unmodified model at $x/d = 7.5$ underpredicts the data by 19%. At $x/d = 8.5$ and 11.5, both models overpredict the data in these surface pressure peaks to within 6% (Figs. 21 and 22).

The rest of this section presents results and discussion on the effect of modification of the turbulence model on two different sized grids. Mesh sizes of $121 \times 89 \times 89$ and $121 \times 159 \times 159$ nodes in the axial $\times$ radial $\times$ circumferential directions were used for the purpose of the grid study. The effect of grid refinement on pitot pressure due to modification is presented at $x/d = 11.5$ in Fig. 23. The effect of grid refinement shows a stronger shear layer and a less elongated shape for the primary vortex. A stronger crossflow shock is captured in the solution with the refined grid. The comparison of eddy viscosity values for the same axial location of $x/d = 11.5$ is also shown in Fig. 23. The values of eddy viscosity are slightly higher for the

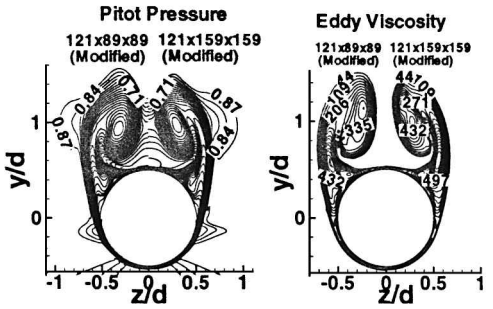


**Fig. 23 Grid study: comparison of pitot pressure and eddy viscosity contours at $x/d$ = 7.5 and 11.5 using modified turbulence model.**

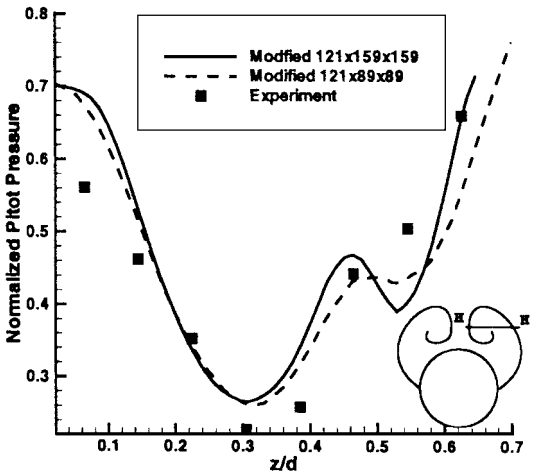


**Fig. 24 Grid study: comparison of pitot pressure along H–H traversing the vortex core, $x/d$ = 11.5.**

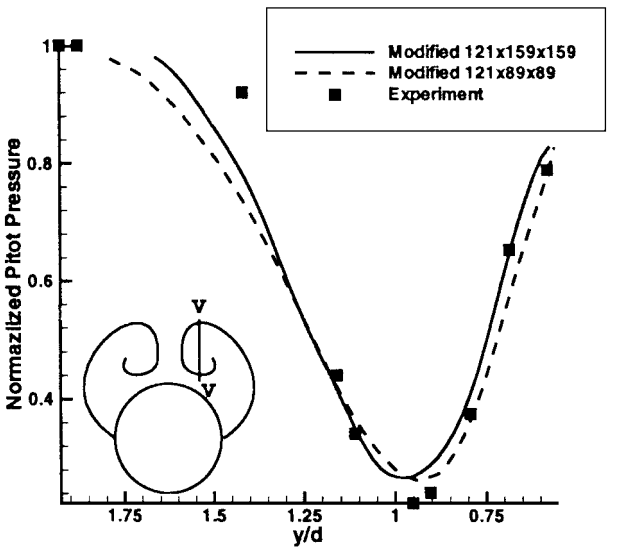


**Fig. 25 Grid study: comparison of pitot pressure along V–V traversing the vortex core, $x/d$ = 11.5.**

refined grid in the vortex, but generally, there is little difference in the magnitude of eddy viscosity due to grid refinement. The effect of grid refinement on pitot pressure along the lines (H–H) and (V–V) through the vortex core at $x/d = 11.5$ are shown in Figs. 24 and 25. Pitot pressure prediction in the vortex core on both grids is the same and underpredicts the data by 19%. The solution on the fine grid matches the data more closely away from the core and also resolves the shear layer better (Fig. 24). The comparison of pitot pressure along the line (V–V) through the vortex core (Fig. 25) shows that the vortex due to the fine grid is less elongated. Figure 23 shows the difference in the vortical structures at $x/d = 11.5$ for the two grids.

## Concluding Remarks

A computational study of supersonic flow past a missile body configuration at an angle of attack is conducted. The flow conditions are Mach number 2.5, $\alpha = 14$ deg, and Reynolds number $1.2 \times 10^6$ based on the cylinder afterbody diameter of 0.09398 m. Accuracy in predictions of surface pressure and pitot pressure in the flowfield was studied for central and upwind difference algorithms and modifications to the $k$–$\epsilon$ turbulence model.

The central and upwind difference methods predicted very nearly the same surface pressures with the maximum difference in surface pressure at $x/d = 11.5$ being 6% for the $Cp$ peak attributed to the crossflow shock. The pitot pressure in the core is overpredicted by the upwind difference method by about 11% compared to the central difference method and experimental data measurement at $x/d = 5.5$.

The effects of modifications to the $k$–$\epsilon$ turbulence model were investigated. Contours of eddy viscosity, pitot pressure, and $x$ vorticity were plotted for comparison purposes. The lowering of eddy viscosity in the vortex improves the prediction of the vortex shape and strength. The improvement in the prediction of the pitot pressure in the core is 15%. The crossflow shock is displaced for the modified case, and this results in better prediction of low-pressure peaks up to $x/d = 6.5$. The modification allows for stronger primary and secondary vortices to be formed, and this results in a more accurate prediction of the low pressure on the surface, e.g., at $x/d = 7.5$, about 19% improvement in the surface pressure prediction of the suction peak attributed to the primary vortex using the modified turbulence model.

Grid resolution studies with the modified turbulence model were conducted. The finest grid considered in this study improved the prediction of the shear layer that rolls up to form the vortex. The finest grid also allowed for prediction of a less elongated vortex at the missile afterbody. There was, however, little variation of surface pressure at all axial stations of the missile body between the grids considered. The overall effect of the modification to the turbulence model is to improve the surface pressure prediction at axial stations up to $x/d = 8.5$ and to improve the shape and strength of the vortex system in the afterbody.

## Acknowledgments

A major part of the computer resources for this work were provided by the Department of Defense High Performance Computing Major Shared Resource Centers, U.S. Naval Oceanographic Office at Bay St. Louis, Mississippi, U.S. Army Corps of Engineers Waterways Experiment Station at Vicksburg, Mississippi, and U.S. Army Research Laboratory at Aberdeen Proving Ground, Maryland. The author is thankful to R. E. Gordnier for help in performing these studies. The experimental data were provided by the Defence Research Agency, United Kingdom.

## References

[1]Degani, D., and Schiff, L. B., "Computation of Turbulent Supersonic Flows Around Pointed Bodies Having Crossflow Separation," *Journal of Computational Physics*, Vol. 66, Sept. 1986, pp. 173–196.

[2]Borrel, M., d'Espiney, P., and Jouet, C., "Supersonic Vortical Flows Around an Ogive-Cylinder," *First European Computational Fluid Dynamics Conference* (Brussels, Belgium), 1992-111, ONERA, Chatillon, France, 1992, pp. 1–8.

[3]Hsieh, T., Priolo, F. J., and Wardlaw, A. B., Jr., "Calculations and Comparisons of the Flowfield About an Ogive Cylinder at $M = 3.5$," *Journal of Spacecraft and Rockets*, Vol. 30, No. 6, 1993, pp. 665–673.

[4]Moran, K. J., and Beran, P. S., "Navier–Stokes Simulations of Slender Axisymmetric Shapes in Supersonic, Turbulent Flow," *AIAA Journal*, Vol. 32, No. 7, 1994, pp. 1446–1456.

[5]Sturek, W. B., Birch, T., Lauzon, M., Housh, C., Manter, J., Josyula, E., and Soni, B., "The Application of CFD to the Prediction of Missile Body Vortices," AIAA Paper 97-0637, Jan. 1997.

[6]Baldwin, B. S., and Lomax, H., "Thin Layer Approximation and Algebraic Model for Separated Turbulent Flows," AIAA Paper 78-0257, Jan. 1978.

[7]Menter, F. R., "Zonal Two Equation $k$–$\omega$ Turbulence Models for Aerodynamic Flows," AIAA Paper 93-2906, July 1993.

[8]Dacles-Mariani, J., Zilliac, G. G., Chow, J. S., and Bradshaw, P., "Numerical/Experimental Study of a Wingtip Vortex in the Near Field," *AIAA Journal*, Vol. 33, No. 9, 1995, pp. 1561–1568.

[9]Gordnier, R. E., "Computational Study of a Turbulent Delta-Wing Flowfield Using Two-Equation Turbulence Models," AIAA Paper 96-2076, June 1996.

[10]Jones, W. P., and Launder, B. E., "The Prediction of Laminarization with a Two-Equation Model of Turbulence," *International Journal of Heat and Mass Transfer*, Vol. 15, No. 2, 1972, pp. 301–314.

[11]Jones, W. P., and Launder, B. E., "The Calculation of Low-Reynolds Number Phenomena with a Two-Equation Model Turbulence," *International Journal of Heat and Mass Transfer*, Vol. 16, No. 6, 1973, pp. 1119–1130.

[12]Gerolymos, G. A., "Implicit Multiple-Grid Solutions of the Compressible Navier–Stokes Equations Using $k$–$\epsilon$ Turbulence Closure," *AIAA Journal*, Vol. 28, No. 10, 1990, pp. 1707–1717.

[13]Sarkar, S., Erlebacher, G., Hussaini, M. Y., and Kreiss, H. O., "The Analysis and Modelling of Dilatational Terms in Compressible Turbulence," *Journal of Fluid Mechanics*, Vol. 227, 1991, pp. 473–493.

[14]Josyula, E., "Computational Study of High-Angle-of-Attack Missile Flows Using Two-Equation Turbulence Models," AIAA Paper 98-0525, Jan. 1998.

[15]Beam, R. M., and Warming, R. F., "An Implicit Factored Scheme for the Compressible Navier–Stokes Equations," *AIAA Journal*, Vol. 16, No. 4, 1978, pp. 393–402.

[16]Jameson, A., Schmidt, W., and Turkel, E., "Numerical Solutions of the Euler Equations by a Finite Volume Method Using Runge–Kutta Time Stepping Schemes," AIAA Paper 81-1259, July 1981.

[17]Roe, P. L., "Approximate Riemann Solvers, Parameter Vectors and Difference Schemes," *Journal of Computational Physics*, Vol. 43, Oct. 1981, pp. 357–372.

[18]Visbal, M. R., "Onset of Vortex Breakdown Above a Pitching Delta Wing," *AIAA Journal*, Vol. 32, No. 8, 1994, pp. 1568–1575.

[19]Rizzetta, D. P., "Numerical Simulation of Turbulent Cylinder Jucture Flowfields," AIAA Paper 93-3038, July 1993.

R. M. Cummings
*Associate Editor*